REPORT DOCUMENTATION PAGE

Form Approved
OMB No. 0704-0188

1. REPORT DATE *(DD-MM-YYYY)*	**2. REPORT TYPE**	**3. DATES COVERED** *(From - To)*
February 2013	Conference Paper	14 Jul 2013 – 19 Jul 2013

4. TITLE AND SUBTITLE
Numerical Analysis of a Single Microchannel Within a High-Temperature Hydrogen Heat Exchanger for Beamed Energy Propulsion Applications

5a. CONTRACT NUMBER
In-House

5b. GRANT NUMBER

5c. PROGRAM ELEMENT NUMBER

6. AUTHOR(S)
Daniel W. Gould, Brad W. Hoff, Marcus P. Young, Rebecca N. Webb

5d. PROJECT NUMBER

5e. TASK NUMBER

5f. WORK UNIT NUMBER
Q0CA

7. PERFORMING ORGANIZATION NAME(S) AND ADDRESS(ES)

Air Force Research Laboratory (AFMC)
AFRL/RQRS
1 Ara Drive
Edwards AFB CA 93524-7013

8. PERFORMING ORGANIZATION REPORT NO.

9. SPONSORING / MONITORING AGENCY NAME(S) AND ADDRESS(ES)
Air Force Research Laboratory (AFMC)
AFRL/RQR
5 Pollux Drive
Edwards AFB CA 93524-7048

10. SPONSOR/MONITOR'S ACRONYM(S)

11. SPONSOR/MONITOR'S REPORT NUMBER(S)
AFRL-RQ-ED-TP-2013-026

12. DISTRIBUTION / AVAILABILITY STATEMENT

Approved for Public Release; Distribution Unlimited

13. SUPPLEMENTARY NOTES
Presented at 2013 ASME Summer Conference on Heat Transfer, Minneapolis, MN; July 14-19, 2013; PA# 13133

14. ABSTRACT

The requirement that the propellants used in launch vehicle systems must also provide the thermal energy to be converted to kinetic energy in the rocket nozzle has plagued rocket designers since the dawn of the space age. Beamed propulsion systems, however, avoid this constraint by placing the energy source on the ground and transmitting the energy to the spacecraft via microwaves. This work computationally models three different heat exchanger channel designs for use in a beam propulsion spacecraft. It was found that despite the very small diameter of the microchannels, each design produced extreme temperature gradients across the channel cross section.

15. SUBJECT TERMS

16. SECURITY CLASSIFICATION OF:			**17. LIMITATION OF ABSTRACT**	**18. NUMBER OF PAGES**	**19a. NAME OF RESPONSIBLE PERSON**
					Marcus P. Young
a. REPORT	**b. ABSTRACT**	**c. THIS PAGE**			**19b. TELEPHONE NO** *(include area code)*
Unclassified	**Unclassified**	**Unclassified**	SAR	8	661-275-6264

Standard Form 298 (Rev. 8-98)
Prescribed by ANSI Std. 239.18

Proceedings of the ASME 2013 Summer Heat Transfer Conference
HT2013
July 14-19, 2013, Minneapolis, MN, USA

HT2013-17217

DRAFT

NUMERICAL ANALYSIS OF A SINGLE MICROCHANNEL WITHIN A HIGH-TEMPERATURE HYDROGEN HEAT EXCHANGER FOR BEAMED ENERGY PROPULSION APPLICATIONS

Daniel W. Gould
University of Colorado Colorado Springs
Colorado Springs, Colorado, United States
Marcus P. Young
AFRL/RQRC
Edwards AFB, California, United States
Brad W. Hoff
AFRL/RDHPS
Kirtland AFB, New Mexico, United States
Rebecca N. Webb
University of Colorado Colorado Springs
Colorado Springs, Colorado, United States

ABSTRACT

The requirement that the propellants used in launch vehicle systems must also provide the thermal energy to be converted to kinetic energy in the rocket nozzle has plagued rocket designers since the dawn of the space age. Beamed propulsion systems, however, avoid this constraint by placing the energy source on the ground and transmitting the energy to the spacecraft via microwaves. This work computationally models three different heat exchanger channel designs for use in a beam propulsion spacecraft. It was found that despite the very small diameter of the microchannels, each design produced extreme temperature gradients across the channel cross section.

INTRODUCTION

Currently the choice of propellants used in launch vehicles is limited by the requirement that the propellants also must provide the thermal energy that is to be converted into kinetic energy in the nozzle. Because of this requirement, modern bi-propellant launch systems must carry both a fuel and an oxidizer such as in the case of the space shuttle, which carries both hydrogen and oxygen. In addition to decreasing the specific impulse of the rocket below that of a system using hydrogen as its only propellant, one must also carry separate tanks, pumps, and plumbing if an oxidizer is to be carried in addition to the fuel. For the past five decades bi-propellant rocket propulsion has been the singular method available to launch large payloads into space. Because of this, bi-propellant rocket designs have already been improved and refined significantly. Therefore, a new method of rocket propulsion is required if any significant gains in rocket performance are to be achieved [1].

The concept of beamed energy propulsion eliminates the need for the propellant to provide its own thermal energy. Rather than increasing the temperature of a gas through chemical reactions between a fuel and an oxidizer, the energy source is kept on the ground and transmitted to the launch vehicle through the use of microwaves or lasers. A wide variety of different beamed energy propulsion concepts exist and the mm-wave energy sources required are technologically feasible. However, in order for this concept to work, a heat exchanger must be designed that can efficiently transmit the heat given by the energy into the hydrogen propellant [2]. This work computationally models a proposed heat exchanger tube for this purpose.

Much work has been done on the design and effectiveness of microchannel heat exchangers for the purposes of cooling electronics [3]. However, these heat exchangers work at far lower temperatures than those that are of interest here. The ultimate goal of this work is to design and characterize a heat exchanger that efficiently absorbs the incoming mm-waves and couples the thermal energy to the hydrogen flow. Temperatures exceeding 2000 K are expected. This paper presents a preliminary feasibility study for a high temperature hydrogen heat exchanger. Only the coupling of the thermal energy to the flow is investigated. Microchannels of three different shapes

are evaluated and the resulting temperatures and velocities from the numerical model are presented.

NOMENCLATURE

T_{max}	=	maximum temperature
V_{max}	=	maximum velocity
T_{ave}	=	mass flow weighted average temperature
ΔP	=	pressure drop
A_{cs}	=	cross-sectional area
A_{rad}	=	area
D_h	=	hydraulic diameter
q''	=	heat flux per unit area
σ	=	Stefan-Boltzmann constant

MODEL

Using the COMSOL Multiphysics 4.3 package, three-dimensional models of all three different heat exchanger tube designs were created. A cross-sectional view of the three tube shapes is shown below Figure 1. All three shapes were sized to have a hydraulic diameter of 1 mm. Each tube is .1 m long and made entirely of the working fluid. As it was assumed that the material that formed the tube walls had an infinite thermal conductivity the solid tube itself was not modeled. The only effect caused by this assumption was that the heat flux was applied directly to the hydrogen rather than to the surrounding solid tube.

In order to analyze the specified situation, the *heat transfer in fluids* and *low Reynolds number k-ε turbulent flow* physics modules were coupled together. This method was found to be more stable than the use of COMSOL's *conjugate heat transfer* physics module. The two physics modules used were coupled simply by setting the heat transfer physics to use the fluid pressure and velocity of the turbulent flow module and setting the turbulent flow module to use the temperature given by the heat transfer module.

Each model consisted of a single tube of hydrogen that was governed by a set of six basic boundary conditions. Three of these constrained the heat transfer felt by the hydrogen while the other three defined the fluid flow. Thus all of the tube's boundaries were constrained by two boundary conditions; one for the heat transfer physics module and one for the turbulent flow physics module.

For the inflow portion of the tube both a constant flow velocity and a constant temperature boundary condition were applied. The magnitude of this velocity was dictated by a mass flow rate requirement of 4.66E-5 kg/s. Set to match the initial temperature of hydrogen as it exits from its storage tank, the constant temperature condition prescribed a temperature of 300 K at the inlet.

For the walls of the tube a no-slip boundary condition was applied in conjunction with a heat flux condition. The value of the heat flux was a two part calculation. First, the incoming heat flux was calculated so that for each shape a total flux of 1.33 kW would be achieved. Next, from this calculated input value the amount of heat lost due to outgoing radiation was subtracted. Here, based on prospective tube shell materials such as carbon fiber reinforced carbon, an emissivity of .9 was chosen. The resultant temperature dependent equation is shown below as Equation 1. In this equation, σ is the Stefan-Boltzmann constant and T is the temperature of the wall at the point where this equation is applied. This equation was used for the cylindrical model. In the other two models, the same basic equation was used but the incoming heat flux term was modified so that design would receive a total of energy input of 1.3 kW before radiative effects are included.

$$q'' = 4.23352E6 - (.9 * \sigma * (T^4 - 300^4)) \qquad (1)$$

Lastly, to the exit of the tube both heat outflow and pressure-no viscous stress boundary conditions were applied. To the latter of these conditions a gage pressure of 0 kPa was set.

Finally, to save time on computation, symmetry boundary conditions were used for the square and triangular cross-sectional tubes. For example, the square tube was cut along its lines of symmetry so that only a quarter of the square remained. Symmetry boundary conditions were then applied to the sides along the lines of symmetry. This method enabled a significantly greater mesh resolution for the same amount of computational time. Figure 1 shows the triangular and square tubes before and after symmetry conditions were used.

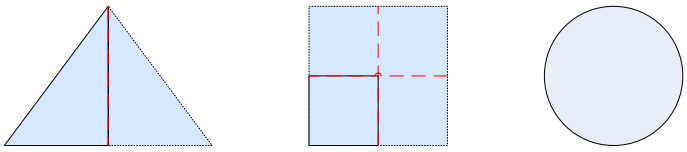

Figure 1 - Tube cross sections after applying symmetry conditions. Here, the solid lines show the final shape, the dotted lines show the removed portions and the red dashed lines show the lines of symmetry used.

After the boundary conditions had been applied to the system, two adjustments were made to the default physics settings. First, the reference absolute pressure in both modules was set to be 1724 kPa, the pressure given by the preliminary design. Second, the heat transfer module was set to use the ideal gas law to calculate the density of the hydrogen.

While COMSOL's material library can provide some of the needed material properties of hydrogen, certain temperature dependent values, such as thermal conductivity and dynamic viscosity, are only given by COMSOL for temperatures up to 1300 K. Because of this, COMSOL's built in hydrogen material data was modified to include material properties for the higher temperatures experienced by the heat exchanger designs evaluated here [4].

For the purposes of these models it was assumed that the hydrogen remained entirely in its diatomic form and did not experience any dissociation due to the high temperatures it was heated to. While the validity of this assumption begins to break down around the maximum temperatures experienced by the hydrogen in these models, due to the limited amounts of the

hydrogen experiencing these maximum temperatures and previous research showing that the amount of atomic – rather than diatomic – hydrogen should be far less than 7% [5], the amount of error resulting from this assumption has been evaluated to be negligible.

Rather than using COMSOL's default mesh, a custom mesh was created for each tube. This was done in three steps. First, the inlet face of the modeled tube was meshed with a triangular mesh. The resolution of the mesh was increased at the outer walls of each tube in order to provide greater detail of the boundary layer. The second step was to sweep the mesh from the inlet face to the outlet face. Finally, the boundary layer mesh feature was also added to the tube to further increase resolution at the tube's outer walls. This custom meshing resulted in meshes of 236800, 244400, and 88000 elements for the square, triangular, and circular tubes, respectively. The lower total element number of the cylindrical model is due to the fact that the axisymmetric model was able to provide much more detail for far less computational time. Thus the axisymmetric model was used for analysis of the cylindrical heat exchanger and the cylindrical three dimensional model was used for comparison only.

The default iterative solver chosen by COMSOL proved to be the most efficient in obtaining a solution for the three-dimensional models. Instead of attempting to solve for each of the dependent variables at the same time, the solution process was broken up into three different segregated steps. In each step the iterative solver was used in conjunction with a multigrid algorithm rather than an Incomplete LU algorithm in order to reduce computational time.

VALIDATION

In addition to the three-dimensional tubes, a two-dimensional axisymmetric model of the cylindrical tube was created. The creation of this model served several purposes. First, by utilizing the axial symmetry of the cylindrical tube in the axisymmetric model the tube could be treated as a two-dimensional - rather than a three-dimensional - problem. This allowed for an extreme increase in mesh resolution for the same computational time as the three-dimensional model. Second, by evaluating the cylindrical tube using both the mesh from the three-dimensional models and the axisymmetric model it was possible to prove that all of the solutions obtained by COMSOL for this particular analysis were mesh independent. Finally, computing both models allowed for validation of the method of using symmetry boundary conditions as was applied to the square and triangular tubes. Significant data from the axisymmetric model is given below in Table 2.

Table 1 - Significant data from the axisymmetric model

	Axisymmetric
T_{max} [K]	2482.6
V_{max} [m/s]	353.4
T_{ave} [K]	1588
ΔP [kPa]	36.3
A_{cs} [mm^2]	.785
A_{rad}[mm^2]	314.16
D_h [mm]	1

RESULTS

Despite the geometric similarity of the models, the results from the numerical analysis showed some significant differences. Significant values from each model are presented below in Table 2.

Table 2 - Significant data from each of the 4 models.

	Square	*Triangle*	*Cylinder*
T_{max} [K]	2590.7	2580	3470
V_{max} [m/s]	276	213	356
T_{ave} [K]	1541	1438	1602
ΔP [kPa]	24.2	15.6	43.5
A_{cs} [mm^2]	1	1.3	.785
A_{rad}[mm^2]	400	519.6	314.16
D_h [mm]	1	1	1

Figure 2, below, shows the velocity profile at the exit of the square tube. Unexpectedly, the maximum velocity did not occur in the middle of the tube (that is, the top right of this symmetrical model) but rather was located in between the tube's center and outer wall. This is explained by the fact that this is a temperature driven flow rather than a pressure driven flow. In a fully-developed pressure driven flow the farther one proceeds from the tube wall across the cross section of the tube the higher the flow's velocity gets. However, in each of the models presented here the driving force behind the flow is temperature rather than pressure. Thus, while the frictional effects experienced by pressure driven flows are still present here, their effect on the velocity profile is partially countered by the nature of the temperature driven flow found here.

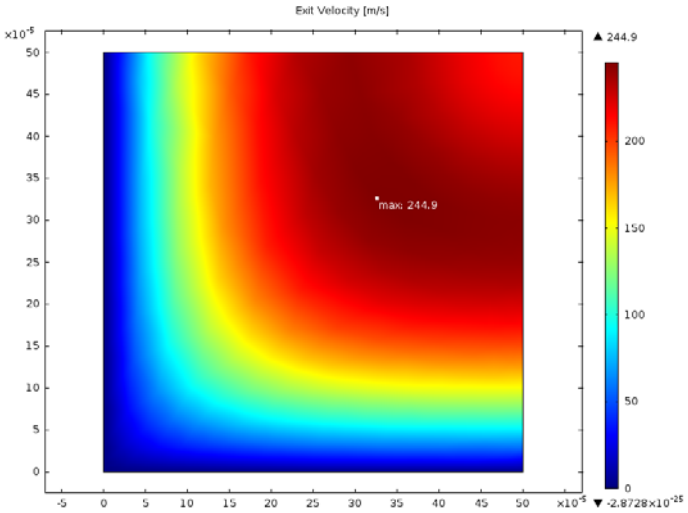

Figure 2 - Velocity profile at exit plane of square model. Note location of maximum velocity.

As the temperature of the hydrogen increases, the density decreases. As the density of the hydrogen decreases, the flow velocity will increase assuming a constant cross-sectional area, as shown by the conservation of mass in Equation 2.

$$\rho_1 A_1 v_1 = \rho_2 A_2 v_2 \quad (2)$$

Thus if frictional effects are ignored, the hottest part of the flow will also be the fastest. As Figure 3 shows, the hottest part of the flow is at the tube walls. The combination of the wall friction and the temperature driven nature of the flow produces a velocity profile in which the point of highest velocity is neither at the center nor at the walls of the tube, but rather lies somewhere in between these two extremes.

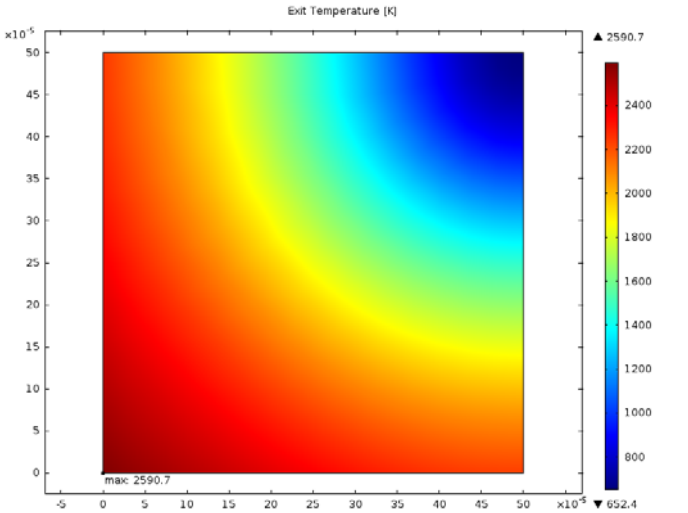

Figure 3 - Temperature at exit of square model.

The results from the triangular model were similar to the results from the square model. As Figure 4 shows, the maximum fluid velocity within the hydrogen is once again positioned between the tube's center and its outer wall. However, unlike the square tube where the maximum velocity occurs at four points around the tube center, the maximum fluid velocity in the triangular tube occurs at three distinct points within the tube.

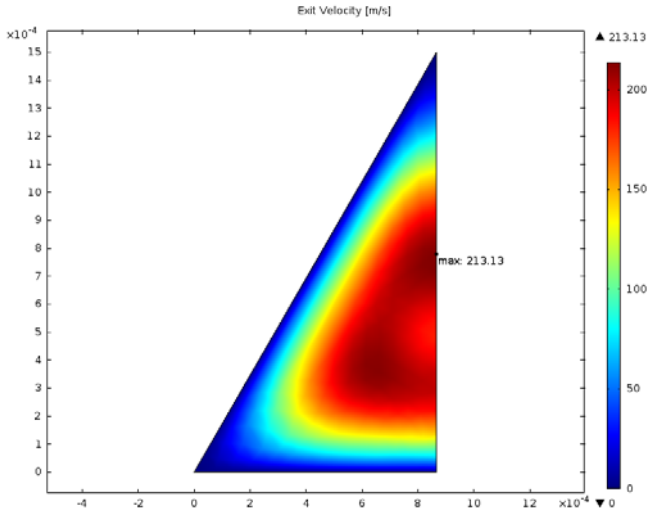

Figure 4 - Velocity of hydrogen at the exit of the triangular tube.

Figure 5 provides the temperature of the hydrogen at the exit of the triangular tube. As expected the tips of the triangle experienced the maximum temperature. While it is expected that if the cross-sectional area of each model had been held constant the maximum temperature of the triangular model would have been higher than that of the square model, due to the fact the hydraulic diameter of each model was chosen to be held constant rather than the area the square model possess the highest maximum temperature.

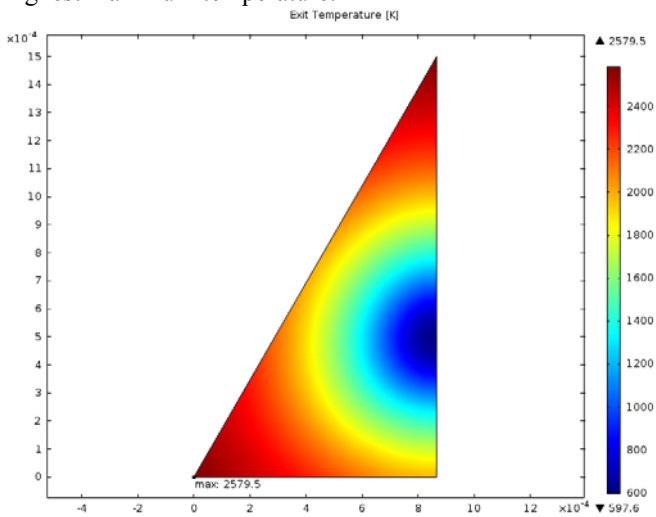

Figure 5 - Temperature at the exit of the triangular model.

Figures 6 and 7, respectively, present the exit velocity and temperature of the three-dimensional cylindrical model. However, as the axisymmetric model offers the same

information as the three-dimensional model but with a much higher accuracy due to the axisymmetric model's far greater resolution, all further discussion of results of the cylindrical tube shape will be restricted to the axisymmetric model.

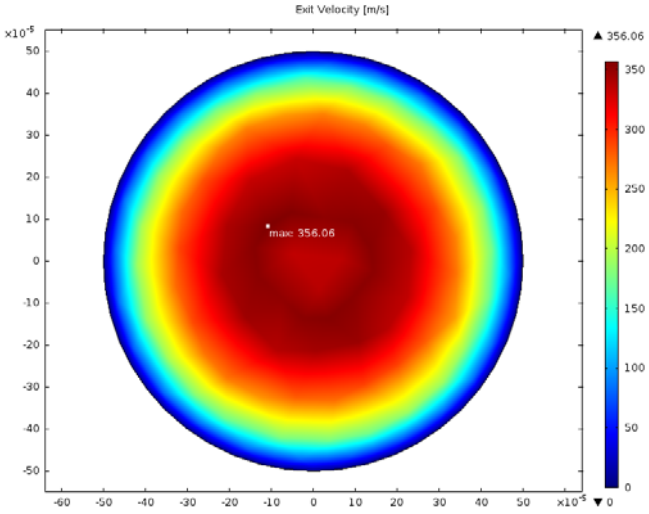

Figure 6 - Fluid velocity at the exit plane of the three-dimensional cylindrical model

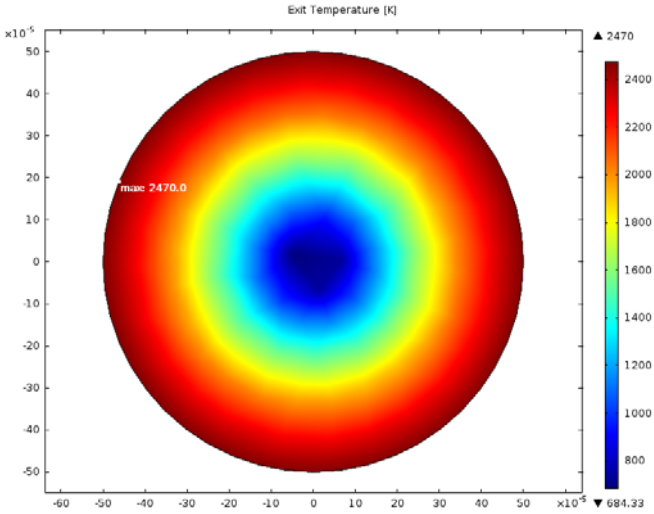

Figure 7 - Fluid temperature at the exit plane of the three-dimensional cylindrical model

Figures 8 and 9 depict the exit velocity and temperature as calculated by the axisymmetric model. It is clearly seen that these figures closely parallel Figures 6 and 7. This similarity both confirms the validity of methods of symmetry used here and also verifies the mesh independent nature of the solutions obtained.

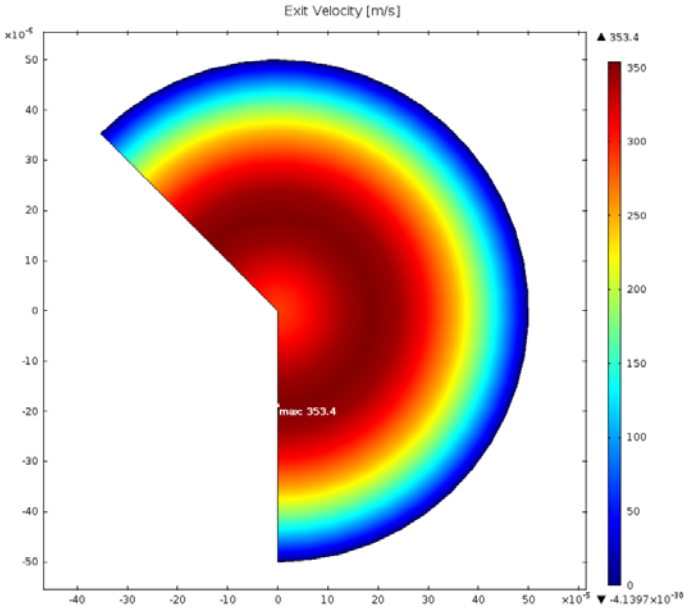

Figure 8 - Fluid velocity at the exit boundary of the axisymmetric model

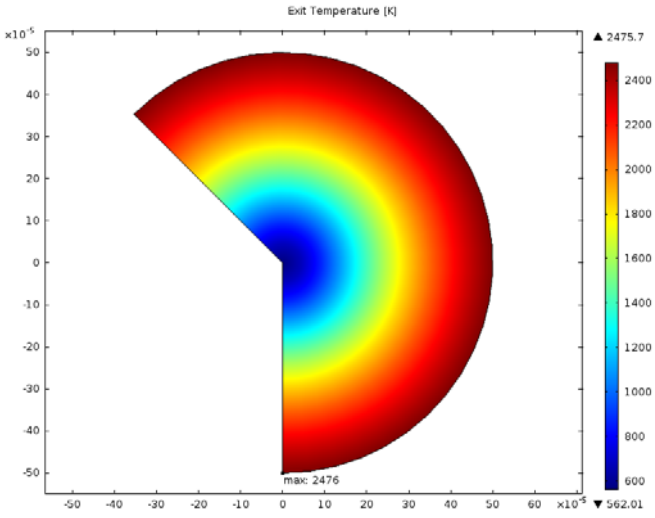

Figure 9 - Fluid temperature at the exit boundary of the axisymmetric model

Figures 10 and 11, respectively, give the cross-sectional temperature and velocity of the fluid as a function of position along the tube length as obtained by the axisymmetric model. In Figure 10, the flat line at 0 m shows the set 300 K temperature at the inlet boundary. The temperature of the system increases with position along the tube. The wall temperature (width = 50E-5 m) increases more rapidly than flow core (width = 0 m) temperatures. Half way down the tube, the wall temperature is 2300 K but the tube center is still at 300 K. At the tube exit, the wall temperature reaches 2500 K but the flow center is at 550 K. The flow velocities and wall effects produce this large gradient. The wall temperature increases are

most dramatic near the tube entrance, increasing 1500 K in the first 0.1 m. Beyond the tube entrance, changes in wall temperature are significantly smaller due to the decreased gradient.

Although a constant inlet velocity boundary condition was used for the inlet boundary conditions on each of the three-dimensional models due to the relative instability of the constant mass flow boundary condition, due to the comparative simplicity of the axisymmetric model the more accurate constant mass flow boundary condition was used. Because of this, the velocity across the entrance – specified as the 0 m line in Figure 11 – is not constant but rather shows a more accurate variance between the center of the tube (width = 0 m) and the tube wall (width = 50E-5 m). This plot clearly shows that everywhere along the tube length, except the tube entrance, the maximum velocity does not occur at the tube center, but somewhere in between the tube center and wall. The location of the maximum moves towards the tube center as the tube exit is neared. This can be attributed to the increased penetration of the heating into the flow with tube length as seen in Figure 10.

Figures 12 and 13 show the temperature and velocity profiles along the length of the tube. In each case, the line marked R = 0 m gives the profile at the center of the tube and the line marked R = .0005 m gives the profile at the tube wall. As expected, Figure 12 shows that the fluid temperature increased fastest and became the highest along the walls of the tube. The wall temperature exceeds 2000 K for over 80% of the tube length. In Figure 13, it can be seen that the velocity trends change beyond a tube length of 0.01 m. Near the entrance, the flow acts like a typical pressure driven flow with the slowest flow at the wall and the velocity increasing towards the center. Beyond the entrance, the flow velocity quickly reaches a maximum at a radius of 2E-4 m. Clearly, the effect of heating is felt by the flow almost immediately.

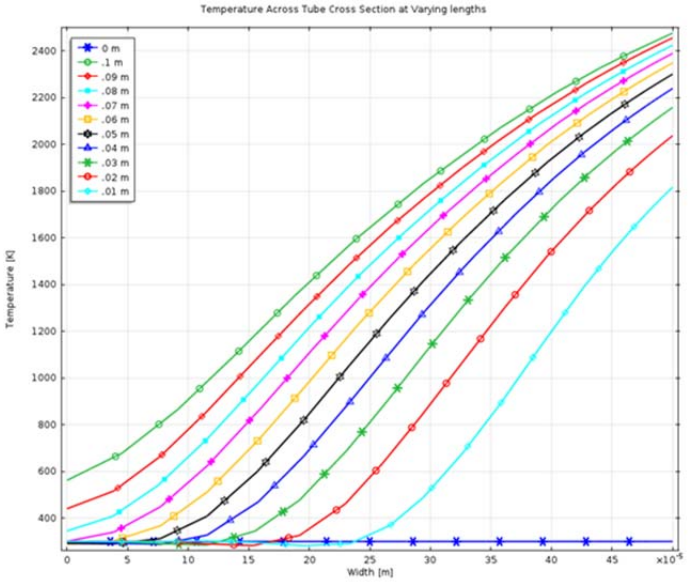

Figure 10 - Hydrogen temperature across cross-section of axisymmetric model

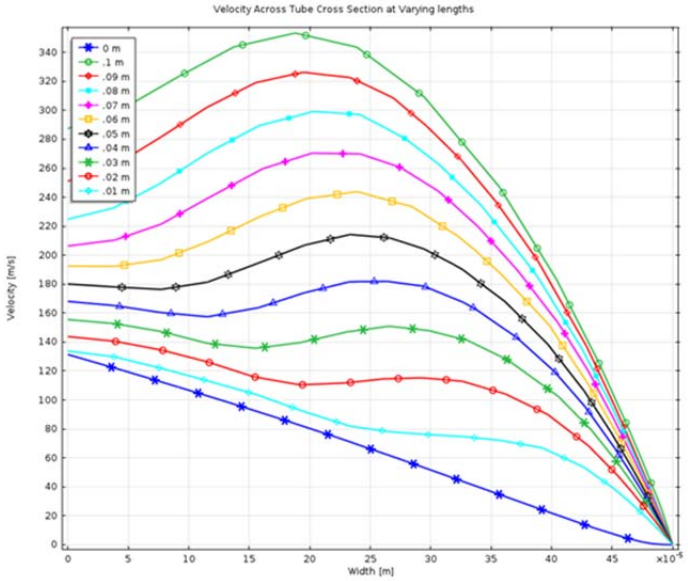

Figure 11 - Fluid velocity across cross-section of axisymmetric model

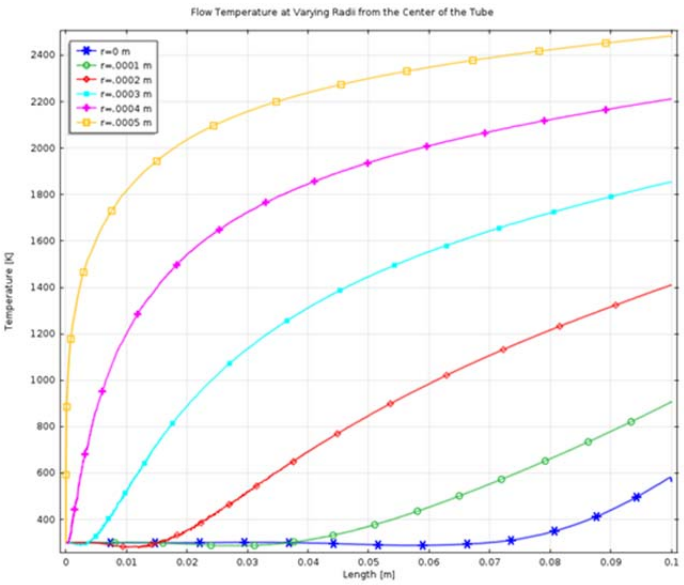

Figure 12 - Hydrogen temperature along the length of the tube

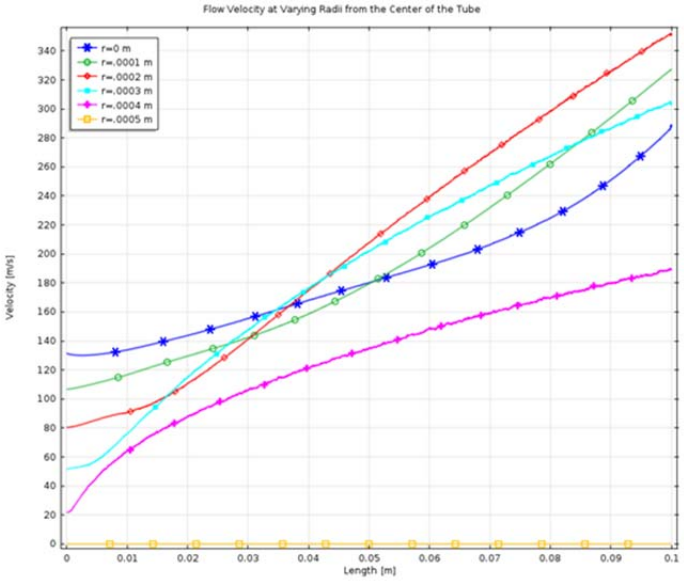

Figure 13 - Fluid velocity along the length of the tube

CONCLUSION

While the models analyzed in this paper may be simple, the numerical study provided several interesting results. First, temperature gradients of almost 2000 K were seen across the radius of each of the three tubes. These extreme gradients were not expected due the tube's microscale radii. Secondly, the velocity profiles produced across the cross section of each shape were not the expected paraboloids. Rather than showing the previously expected exponential rise in velocity from its minimum at the tube wall to its maximum at the tube center, each model's velocity profile placed the maximum fluid velocity at a location in between the tube center and wall.

ACKNOWLEDGMENTS

This work is funded by SAIC Inc.

REFERENCES

[1] Parkin K., 2006, "THE MICROWAVE THERMAL THRUSTER," **2006**(May).

[2] Murakami, D.D. and Parkin, K.L., 2012, "An Overview of the NASA Ames Millimeter-Wave Thermal Launch System," ARC-E-DAA-TN5645, NASA.

[3] Yang Y., Brandner J. J., and Morini G. L., 2012, "Hydraulic and thermal design of a gas microchannel heat exchanger," Journal of Physics: Conference Series, **362**, p. 012023.

[4] Yos J., 1963, "Transport properties of nitrogen, hydrogen, oxygen, and air to 30,000 K," pp. 26–27.

[5] Greenwood N. N., and Earnshaw A., 1998, "Chemistry of the Elements (2nd Edition)," p. 35.

